Optical darkness in short-duration γ-ray bursts

Caden Gobat[1,2,⋆], Alexander J. van der Horst[1], David Fitzpatrick[3,4]

[1]*Department of Physics, George Washington University, 725 21st St NW, Washington, DC 20052, U.S.A.*

[2]*Department of Space Operations, Southwest Research Institute, 1050 Walnut Street, Suite 300, Boulder, CO 80302, U.S.A.*

[3]*Department of Aerospace Engineering Sciences, University of Colorado Boulder, 3775 Discovery Dr, Boulder, CO 80303, U.S.A.*

[4]*Department of Physics, Georgetown University, 37th & O St NW, Washington, DC 20007, U.S.A.*

ABSTRACT

Gamma-ray bursts categorically produce broadband afterglow emission, but in some cases, emission in the optical band is dimmer than expected based on the contemporaneously observed X-ray flux. This phenomenon, aptly dubbed "optical darkness", has been studied extensively in long GRBs (associated with the explosive deaths of massive stars), with possible explanations ranging from host environment extinction to high redshift to possibly unique emission mechanisms. However, investigations into optical darkness in short GRBs (associated with the mergers of compact object binaries) have thus far been limited. This work implements a procedure for determining the darkness of GRBs based on spectral indices calculated using temporally-matched *Swift*-XRT data and optical follow-up observations; presents a complete and up-to-date catalog of known short GRBs that exhibit optical darkness; and outlines some of the possible explanations for optically dark short GRBs. In the process of this analysis, we developed versatile and scalable data processing code that facilitates reproducibility and reuse of our pipeline. These analysis tools and resulting complete sample of dark short GRBs enable a systematic statistical study of the phenomenon and its origins, and reveal that optical darkness is indeed quite rare in short GRBs, and highly dependent on observing response time and observational effects.

Key words: gamma-ray bursts – neutron star mergers – dust, extinction – methods: observational

1 INTRODUCTION

Gamma-ray bursts (GRBs) are some of the brightest transient astrophysical phenomena observed in the Universe. The prevailing hypothesis is that GRBs are the products of two main classes of progenitors: collapsar events, resulting from end-of-life core collapse in supermassive stars (Woosley 1993), or compact object (neutron star-neutron star or possibly neutron star-black hole) binary mergers (Eichler et al. 1989). Observationally, GRBs are generally split into sub-populations corresponding to these two progenitor types on the basis of the burst's T_{90} duration (see Kouveliotou et al. 1993), the time it takes for it to emit 90% of its gamma-ray radiation. Short GRBs, typically associated with binary neutron star (BNS) mergers,[1] are usually taken to be those with $T_{90} \lesssim 2$ seconds, and long GRBs, resulting from core collapse events, are those with $T_{90} \gtrsim 2$ seconds. When available, other metrics can be used to classify GRBs as well, such as spectral hardness and luminosity (short GRBs are typically spectrally harder but less luminous than long ones). For an in-depth review of gamma-ray bursts, see Gehrels et al. (2009).

Categorically, after the initial burst, called prompt emission, GRBs produce an afterglow, which refers to a period of fading multi-wavelength emission that lasts from hours to days and sometimes

years after the initial event. In 1997, van Paradijs et al. announced the discovery of the first optical counterpart to a GRB, and transient optical afterglows have been identified from many GRBs since. Shortly after the initial discovery, however, Groot et al. (1998) reported on the discovery of a GRB with no detectable optical afterglow. Since then, observers have found that a fraction of all GRB afterglows exhibit a phenomenon known as optical darkness, where the afterglow as a whole is clearly detected (typically in the X-rays) and yet much dimmer than expected or not present at all in the optical band. This phenomenon has been observed in both long and short GRBs (Greiner et al. 2011), with a number of proposed explanations (Fynbo et al. 2001). However, the implications of optical darkness differ somewhat for the two different classes of progenitor.

The massive stars associated with long GRBs live fast and die young, while the compact object binaries that give rise to short GRBs must be old enough for both members to have gone supernova and turned into neutron stars, and then orbit each other for long enough to spiral inwards and collide. One possible cause of optical darkness in some GRBs is that emission has been redshifted towards the infrared due to cosmological distance and the expansion of the Universe, but this would imply that the event occurred long ago, when the Universe was relatively young. This explanation makes sense for long GRBs, which can reasonably be expected to be possible within ~ 1 Gyr after the Big Bang. However, compact binary merger events should not be expected to occur often at this early stage of the Universe's evolution, as it is unlikely that they would have had time to form (Zheng & Ramirez-Ruiz 2007; Wanderman & Piran 2015; Beniamini & Piran

---

⋆ E-mail: cgobat@gwu.edu

[1] Observational confirmation that BNS mergers are linked to short GRBs came with the simultaneous observation of kilonova AT2017gfo, GRB 170817A, and gravitational wave event GW170817 (LIGO Scientific Collaboration et al. 2017).

2019; Skúladóttir & Salvadori 2020). Another proposed explanation is host galaxy extinction (Lazzati et al. 2002; Covino et al. 2013; Littlejohns et al. 2015), which refers to the possibility that gas and dust within the galaxy where the GRB occurred blocks light in the optical band. Again, this is rational for long GRBs, which occur in regions of star-forming activity amidst environments of dense gas and dust. However, this is not so universally applicable for short GRBs, whose progenitors often travel far away from where the stars formed (e.g., Berger 2010; O'Connor et al. 2022), and are not as predictably found in these kinds of regions. A final explanation is that optical darkness is an intrinsic property of certain GRBs: some simply might not emit as much optical light as others. However, this unique physics explanation is disfavored, at least for long GRBs (Rol et al. 2005). Partly as a result of these contrasts, and partly due to the overall difference in afterglow brightness of long and short GRBs, optical darkness in long GRBs has been studied much more extensively than in short ones. In this work we focus on short GRBs in order to better understand the environments in which they form and the histories of the systems that produce them.

There are two main criteria in the literature for determining if a burst is optically dark, and both depend on the optical-to-X-ray spectral power-law index, β_{ox}, which provides a metric for the relative flux intensity at X-ray versus optical frequencies. In general, a low value of β_{ox} means that the power-law slope between the optical and X-rays is shallow, or perhaps even positive (we utilize the sign convention of $F_\nu \propto \nu^{-\beta}$, meaning $\beta < 0$ implies a positive slope and consequently higher emission in the X-rays than in the optical). The first method (Jakobsson et al. 2004) defines optical darkness with a cutoff of $\beta_{ox} < 0.5$, which is derived from the assumption that the number distribution of electron Lorentz factors in the burst outflow (described by $n_e(\gamma) \propto \gamma^{-P}$) is limited by $p > 2$. Integrating the synchrotron emission produced by such an electron distribution results in a lower limit of $\beta > 0.5$ on the broadband spectrum, meaning violations of this should be considered abnormal (i.e., "dark"). However, cases of $p < 2$ have been found (e.g., Masetti et al. 2001; Stanek et al. 2001), so this assumption is not universally valid.

The second method (van der Horst et al. 2009) incorporates a burst's X-ray spectral information, which is routinely available thanks to the rapid follow-up capabilities of the Neil Gehrels *Swift* Observatory (hereafter *Swift*) and its X-ray Telescope (*Swift*–XRT, Burrows et al. 2005). If the spectral index in the X-ray regime (β_x) is known, it can be compared to the optical-to-X-ray spectral index. van der Horst et al. define a burst as optically dark if $\beta_{ox} < \beta_x - 0.5$, allowing for the possibility that $p < 2$. Given current physical models for GRB afterglow emission mechanisms, and assuming that the optical and X-ray emission are part of the same broadband spectrum, all bursts should in theory lie in the region $\beta_x - 0.5 < \beta_{ox} < \beta_x$, meaning that if β_{ox} is below this range, the burst is optically dark.

This work implements a scalable pipeline for determining darkness using both of these methods, with special care given to sample completeness and systematic procedures for retrieval of X-ray spectra and light curves, as well as ultraviolet (UV), optical, and near-infrared (nIR) follow-up observations. Using this, we present a complete catalog of optically-dark short GRBs since *Swift*'s launch in 2004 through the end of 2021, which offers insight into the mechanisms and possible causes of the phenomenon.

In Section 2, we present the methodology, sample selection and pipeline we developed for this work. We show the results in Section 3, and discuss the implications for the entire short GRB population and a few interesting cases in Section 4. Section 5 summarizes and concludes this paper.

2 METHODOLOGY & PIPELINE

To determine β_{ox} for a given GRB, we first require the existence of time-resolved flux data in both the optical/nIR/UV and X-ray bands for comparison. Multi-wavelength data must also be relatively coincident in time to make a valid comparison, due to the afterglow's rapid temporal decay. We also require existing X-ray spectral fits, given that the van der Horst et al. (2009) criterion for optical darkness depends on β_x, the X-ray spectral index.

To accomplish this, we implemented a mostly automated data reduction and analysis pipeline in Python, with several distinct, consecutive sections. X-ray flux data and spectral information are retrieved automatically from online repositories as a part of this process, while optical data is compiled manually. The code searches for temporal matches between these two data sets for each burst within a user-defined tolerance, and calculates β_{ox} using appropriately converted fluxes that have been corrected for Galactic extinction.

2.1 Sample definition and data collection

Our sample definition starts from the master-level *Swift* GRB table, with updated T_{90} values pulled from the *Swift* Burst Alert Telescope catalog pages. From there, we select all GRBs up through the end of 2021 that meet one or more of the following criteria:

- $T_{90} \leq 2$ seconds;
- present in the sample of Fong et al. (2015), whose criteria were:

  – occurrence between November 2004 and March 2015, and
  – $T_{90} \lesssim 2$ seconds, with exceptions made for GRBs 050724A, 090607 and 100213A (which have T_{90} between 2.5 and 3 seconds) on the basis of spectral lag/hardness ratio, and
  – follow-up observations in the X-ray, optical, near-infrared, or radio bands are available.

- present in the sample of Rastinejad et al. (2021), whose criteria were:

  – occurrence between 2005 and 2020, and
  – detected by *Swift*–BAT, and
  – $T_{90} \lesssim 2$ seconds, or classified as short in the *Swift*–BAT catalog (Lien et al. 2016).

- GCN Circular announcement(s)[2] for the burst identify it as short.[3]

This results in a master table with a list of GRB identifiers as well as basic information about the bursts.

The calculation of β_{ox} requires contemporaneous flux measurements in the X-ray and optical bands. The UK *Swift* Science Data Center (UKSSDC; Evans et al. 2007, 2009) provides X-ray data taken by *Swift*–XRT. To collect these data, we wrote custom retrieval scripts to query the online repository to scrape each burst's spectrum page[4] for its X-ray photon index, Γ (from which we get the X-ray spectral index using the relationship $\Gamma = 1 + \beta_x$), and intrinsic column density, N_H. We parse the lightcurve page[5] to obtain an X-ray

---

[2] https://gcn.gsfc.nasa.gov/selected.html

[3] The process for identifying these bursts was partially automated, and GCN Circular scraping code can be found on GitHub at cgobat/dark-GRBs/GCNs.ipynb and cgobat/dark-GRBs/catalog generator.ipynb

[4] https://www.swift.ac.uk/xrt_spectra/

[5] https://www.swift.ac.uk/xrt_curves/

flux time series, and the XRT Live Catalog pages[6] for fitted temporal indices (α) and corresponding light curve break times.

The majority of our optical, nIR, and UV data were parsed and compiled manually from GCN Circular announcements of follow-up observation results for GRBs of interest, plus data presented in peer-reviewed publications. In recent years, GRB localizations published through the GCN have enabled increasingly frequent and rapid follow-up observations by telescopes around the world. By compiling data from the GCN Circulars for each of the bursts in our sample, we compile a table of magnitudes of optical detections, upper limits, and associated errors, as well as the observation time and observing instrument/band. We supplement these data with the short GRB optical observations presented in Fong et al. (2015) and Rastinejad et al. (2021).

2.2 X-ray data processing

The UKSSDC provides *Swift*-XRT light curves for GRBs in units of integrated flux across the entire XRT 0.3–10 keV band. To compare fluxes at specific wavelengths, it is necessary to convert these integrated fluxes into spectral flux densities (i.e., units of Jy or similar). Within the X-ray band, we assume the afterglow spectrum (as a function of frequency, ν) to be described by a single power law with spectral index $\beta_{\rm x}$. This yields the following relation:

$$F_{\rm x} = \int_{0.3\,\text{keV}}^{10\,\text{keV}} F_E \, dE = A \int_{7.3 \cdot 10^{16}\,\text{Hz}}^{2.4 \cdot 10^{18}\,\text{Hz}} \nu^{-\beta_{\rm x}} \, d\nu \tag{1}$$

where $F_{\rm x}$ is the bolometric X-ray flux value from *Swift*-XRT and A is a scaling coefficient that accounts for intrinsic X-ray luminosity and distance to the burst. The value of A can be determined via the analytical solution to Eq. (1), which is

$$F_{\rm x} = A \cdot \begin{cases} \ln(\nu) & \text{if } \beta_{\rm x} = 1 \\ \frac{\nu^{1-\beta}}{1-\beta} & \text{otherwise} \end{cases} \Bigg|_{\nu=7.3 \cdot 10^{16}\,\text{Hz}}^{\nu=2.4 \cdot 10^{18}\,\text{Hz}} \tag{2}$$

We can thus evaluate $A\nu^{-\beta_{\rm x}}$ at $\nu = 10^{\frac{\log(10)+\log(0.3)}{2}} \approx 1.732$ keV, the logarithmic midpoint frequency of the 0.3–10 keV range, to get $F_{\nu,\rm x}$, the spectral flux in the logarithmic middle of the X-ray band. We perform this computation for every entry in the XRT data table (on the order of several tens of data points for each GRB) to compute a usable spectral flux for each flux data point.

2.3 Optical data processing

Information collected in the optical regime includes observation time, magnitude or limiting magnitude, magnitude error, observation filter and its effective wavelength $\lambda_{\rm eff}$, and the Galactic reddening E_{B-V} in the direction of the GRB. For the most part, magnitudes are reported in the AB system. Where Vega magnitudes are reported, as in the case of the *Swift* UV/Optical Telescope (UVOT, Roming et al. 2005), we apply a correction factor to translate into AB magnitudes.[7]

The extinction at some wavelength λ is given by $A_\lambda = R_\lambda \cdot E_{B-V}$, where R_λ is dependent on λ and E_{B-V} is an observed property of the interstellar medium along the line-of-sight. To calculate this $R(\lambda)$ for Galactic extinction, we establish an interpolatory function using empirical extinction data provided in Schlafly & Finkbeiner (2011)'s Table 6. The relationship is well-defined, as shown in Figure 1.
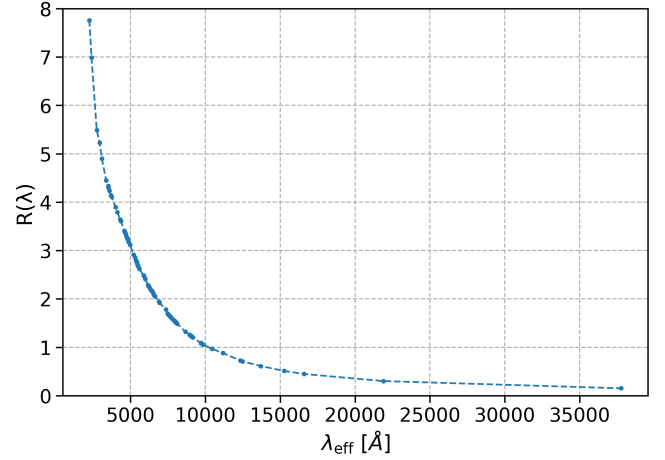
Figure 1. Relationship between an observing filter's effective wavelength and coefficient R_λ that we use to convert between E_{B-V} reddening and magnitude extinction.

Knowing this and the reddening value for each GRB, we calculate the Galactic extinction and adjust our magnitude values for it. With all of this information, we then calculate a spectral flux or upper limit for the observation according to

$$F_{\nu,\rm o} = 3631 \cdot 10^{-\frac{m_\lambda - A_\lambda}{2.5}} \text{ Jy} \tag{3}$$

2.4 Temporal matching & calculation of $\beta_{\rm ox}$

With unit-compatible flux values in the X-ray and optical bands, the next step is to match these data points in time. We define the fractional temporal separation between optical observation time ($t_{\rm o}$) and X-ray observation time ($t_{\rm x}$) as

$$dt_{\%} = \frac{|t_{\rm o} - t_{\rm x}|}{t_{\rm x}} \tag{4}$$

and compute this for every combination of optical and X-ray data points within each GRB, accepting any pair of data points for which $dt_{\%} \leq 0.2$ as a candidate match.

For each temporal match of X-ray and optical data, we calculate $\beta_{\rm ox}$, the power-law slope between the two points:

$$\beta_{\rm ox} = -\frac{\log(F_{\nu,\rm x}/F_{\nu,\rm o})}{\log(\nu_{\rm x}/\nu_{\rm o})} \tag{5}$$

Because this calculation assumes exactly contemporaneous flux observations in the two bands, we must also account for some additional error due to time-dependent afterglow decay. If the afterglow is fading rapidly, even a small difference in time could correspond to a notably different flux. We use the X-ray temporal decay index α (defined such that $F_{\rm x}(t) \propto t^{-\alpha}$; also retrieved from the UKSSDC online repository) to calculate the error due to the separation in time that does exist. This additional temporal error is determined using the formula

$$\Delta\beta_{\rm ox} = |\alpha \log(1 + dt_{\%})| \tag{6}$$

and then combined with the propagated uncertainty on $\beta_{\rm ox}$. For each matched pair and resultant $\beta_{\rm ox}$, we set a boolean flag for optical darkness according to the Jakobsson et al. method if $\beta_{\rm ox} < 0.5$, and for the van der Horst et al. method if $\beta_{\rm ox} < \beta_{\rm x} - 0.5$.

2.5 Uncertainty handling & error propagation

All stages of the pipeline described above involve quantities with associated uncertainties. In many cases, this uncertainty is asymmetric (i.e., the error in the positive direction differs from the error in the negative direction). To ensure proper handling and propagation of all of these uncertainties, we utilize the `asymmetric_uncertainty` software package (Gobat 2022), a stand-alone Python library for representing such numbers. The package's main functionality lies in its implementation of a novel object type for representing quantities of the form $\mu_{-\sigma_-}^{+\sigma_+}$, where μ is the expected value and $\sigma_\pm$ are (not necessarily equivalent) uncertainties in the positive and negative direction. Instances of this class class behave appropriately under all standard mathematical operations (addition, division, exponentiation, etc.), and can be combined with one another (or other numerically-typed objects) using such operations to propagate their associated uncertainties. Mathematically, each object is treated as two conjoined and jointly normalized halves of a Gaussian probability distribution (as introduced by John 1982), with a PDF P described by

$$P(x, \mu, \sigma_-, \sigma_+) = \frac{\sqrt{2}}{\sqrt{\pi}(\sigma_- + \sigma_+)} \cdot \begin{cases} \exp\left(-(x-\mu)^2/2\sigma_-^2\right) & x < \mu \\ \exp\left(-(x-\mu)^2/2\sigma_+^2\right) & x > \mu \end{cases}$$

(7)

where x is the independent random variable, μ is the x-coordinate of the peak, and $\sigma_\pm$ independently set the width to either side of that peak.

Notable examples of quantities involved in this analysis that have asymmetric uncertainties are the X-ray flux F_x, observation time t_x, and spectral index β_x. This means that each β_{ox} ends up with an asymmetric uncertainty, since its calculation depends upon all of the aforementioned values. The software is also capable of handling classical (symmetric) uncertainties ($\sigma_+ = \sigma_-$), as well as upper/lower limits (using variations on $\texttt{nominal}_{-\infty}^{+0}$ or $\texttt{nominal}_{-0}^{+\infty}$, respectively), making it a versatile computational tool.

3 RESULTS

The original sample of short *Swift* GRBs consists of 193 events, spanning from February 2005 through the end of 2021. Of these, there is an X-ray light curve for 163 and at least one optical observation for 165. The overlap between these two sets (i.e., the number of bursts for which there are both X-ray and optical data) is 145. Of the latter, 108 bursts have at least one temporally matching set of data points with $dt_\% \leq 0.2$, which comes out to 6.5 ± 0.5 candidate short GRBs per year of the sample. Finally, 54 bursts have at least one match that qualified as optically dark by at least one of the methods described above, yielding an average rate of 3.2 ± 0.4 empirically dark short bursts per year. These numbers give a rate of approximately $49\% \pm 7\%$ of eligible bursts that are nominally dark (at some point) by one or both methods. The number of bursts per year is shown in Figure 2.

However, the vast majority of these optically dark points come from very early-time follow-up observations. We can observe this effect in our sample of short GRBs as a whole by studying the time distributions of optical/X-ray observation pairs that qualify as dark versus not dark points. The number of bursts that qualify as dark, broken down into discrete classification of observation times (< 5, $5 - 50$ and > 50 minutes) and the breakdowns are given in Table 1, showing a clear trend between darkness classification and time after burst. Continuous distributions of observation times split by darkness classification are shown in Figure 3.
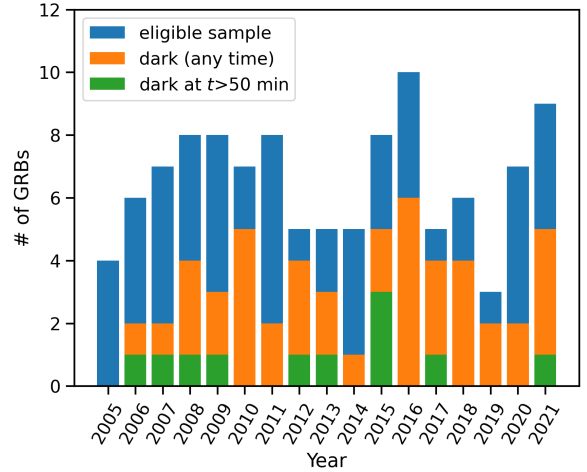

Figure 2. Bursts per year in our sample as a whole as compared to bursts per year that have at least one matched data pair that qualifies as dark by one or both methods.

t_o	Not dark	Dark
<5 min	39	58
5–50 min	205	68
>50 min	680	26

Table 1. Darkness classification (by one or both methods) of temporally-matched observations across all GRBs, broken down by optical observation time, showing that early-time observations are disproportionately dark.
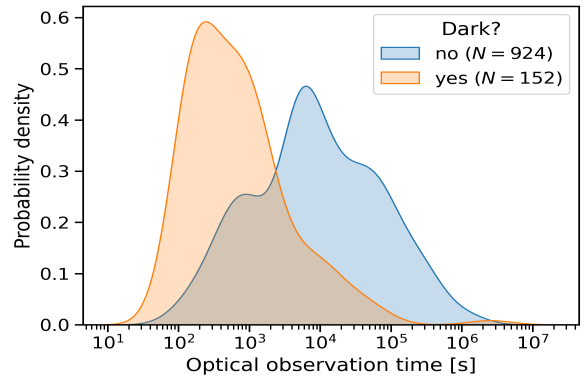

Figure 3. Kernel density plot showing the distribution of all optical observation times for dark data pairs and not dark data pairs. These distributions are not analogous, confirmed by a Kolmogorov-Smirnov (K-S) test statistic of $D = 0.58$ with $p \approx 0$, which demonstrates with very high confidence that the two do not come from the same parent distribution.

To illustrate this effect quantitatively, we perform a search for events that have a calculated dark point at later times. We find 23 such bursts with a dark point beyond 5 minutes (300 seconds) after the start of the prompt gamma-ray emission, and only 10 with an optically dark point beyond 50 minutes (3000 seconds).

A complete summary of the resultant products of this work is visualized in Figure 4, which shows the distributions of β_x and β_{ox} relative to one another for the darkest (lowest value of β_{ox}) matched data pair for each GRB. This plot may therefore skew somewhat 'dark', as it has not been corrected for the early-time anomalies dis-

cussed above. Interestingly, we note that the location of the apparent peak in the distribution of β_{ox} lies just below 0.5, which is Jakobsson et al.'s cutoff for defining optical darkness.

4 DISCUSSION

Our preliminary finding that just under half of short bursts exhibit optical darkness is unexpected, as previous studies (Rol et al. 2005; Greiner et al. 2011; Littlejohns et al. 2015) have found a similar fraction for long GRBs. Due to the general differences in the environments and redshifts at which we expect short versus long GRBs to occur, it is surprising to find similar rates of optical darkness between the two populations. There are a number of possible reasons for this unexpected initial result.

4.1 Early-time X-ray emission

Swift's short response time, in combination with the number of currently operational ground-based observatories capable of performing rapid follow up, often results in simultaneous observational coverage of GRB afterglows in the optical and X-ray bands. Because it is possible for afterglow emission in the X-ray and optical bands to fade over time at different rates (Greiner et al. 2011), the resulting value of β_{ox} can change over time as well, even over the course of a single burst's afterglow.[8] This could be due to the optical and X-ray regimes being in different parts of the same broadband spectrum, or two different emission components contributing to the observed optical and/or X-ray emission.

As discussed in §3, we note numerous cases where a burst qualifies as dark at early times, but not at later times. To investigate the effects of observation time on perceived optical darkness, we inspected the light curves of individual dark bursts and noted that many such points where $\beta_{ox} < 0.5$ or $\beta_{ox} < \beta_x - 0.5$ (or both) coincide with times when there is clearly atypical behavior occurring in the X-rays. The canonical behavior for the temporal evolution of the X-ray afterglow (Nousek et al. 2006) is a brief period of very steep decay ($\alpha \approx 3$), followed by a shallow decay ($\alpha \approx 0.5$), and then finally a decay with an intermediate slope ($\alpha \approx 1.0$–1.5). When the observed light curve behavior differs significantly from the latter, intermediate slope, our assumption about how the X-rays should behave is violated in comparison to the optical band, since there may be multiple emission components at play. Therefore, we hypothesize that many of these early points are dark by technicality, but not necessarily because of low optical flux; an X-ray excess is just as capable of causing β_{ox} to be shallow. The lightcurves of GRBs 161004A and 170822A (Figure 5) provide particularly notable examples of this, with an early X-ray flare and an extended plateau, respectively.

We conclude that although many bursts may qualify as optically dark in the numerical sense, it is often not in the interesting sense of the phenomenon that we seek. There are a number of possible reasons for this anomalous X-ray behavior at early times (Nousek et al. 2006; Liang et al. 2006). There is a chance that early X-ray observations are catching the tail end of the burst's prompt emission or prolonged central engine activity. Regardless of whether the merger product is a rapidly spinning supra-massive neutron star or collapses immediately into a black hole, we expect that not all of the matter

from the two progenitor objects will be consumed immediately: there is likely a short-lived accretion disk still actively fueling relativistic jets within the first few seconds or minutes after the burst. The current physical understanding of GRB afterglows is that emission arises from external shocks between the burst outflow and material in the surrounding environment. To explain the extra emission in the X rays, we need an additional emission component beyond a standard forward shock afterglow model, and this could be the result of a number of theorized mechanisms, including prolonged central engine activity, stratified ejecta, or a reverse shock scenario. This is because there are also interactions within the jet structure that must be considered: for example, a faster-moving blast wave behind the main shock front may eventually catch up with it and inject additional energy. Once this has all played out, however, we observe the X-ray light curves settle into more typical behavior in time.

4.2 Short GRBs with extended emission

Because of our sample selection methodology, there are a number of sample members that do not obey the $T_{90} \leq 2$ second criteria. In fact, some have prompt durations on the order of tens or hundreds of seconds. These are bursts with extended emission (Norris & Bonnell 2006), where high-energy emission continues beyond the main peak of the burst. An open question is what sets these bursts apart and why. Figure 6 shows the distribution of our sample in T_{90} space. Of note is the presence of two separate peaks that each appear to be distinct log-normal distributions, which reaffirms that our sample selection methodology is reasonable, and suggests the possibility that short bursts with extended emission (EE) form a distinct class with a different physical origin than typical short GRBs.

To probe whether these EE bursts arise from a different physical process, we examined the rates of optical darkness and late-time optical darkness on either side of the T_{90} cutoff. We count the number of bursts on either side of this split and compare the relative fractions of bursts that possess optically dark data points as well as bursts with dark data points at late times (i.e., $\delta t > 5$ minutes). If we find significantly different fractions of optical darkness or late-time optical darkness, we might infer that EE bursts (those in our sample but with comparatively large values of T_{90}) might be physically distinct from typical short bursts in their origins. The results of this analysis are shown in Table 2. While these numbers may hint at EE bursts being more optically dark than non-EE short bursts, when we incorporate and propagate uncertainties (Poisson statistics; $\sigma_N \approx \pm\sqrt{N}$), the fractions' errors overlap at the 1.5–2σ level, meaning no significant conclusion can be drawn.

A reanalysis of *Swift*–BAT lightcurves by Dichiara et al. (2021) found that a majority of sGRBs at high redshift ($z \gtrsim 1$) display extended emission, despite often having a measured T_{90} of ≤ 2 s. They note the possibility that this is due to EE bursts arising from progenitors other than binary neutron star mergers. Other studies (Troja et al. 2008; Gompertz et al. 2020) have suggested that EE short bursts are the result of neutron star-black hole binary mergers, as opposed to mergers of binary neutron stars. This is supported by physical modeling, as well as the fact that EE bursts are typically found closer to their host galaxies than non-EE bursts (O'Connor et al. 2022). This is notable because if true, it could reasonably be expected to contribute to optical darkness as well. Although our results hint at this possibility, larger number statistics are required to support or refute this.

---

[8] If the temporal decays of the optical and X-rays paralleled one another exactly, the two light curves would always be the same distance apart in logarithmic space, resulting in a constant value of β_{ox}.
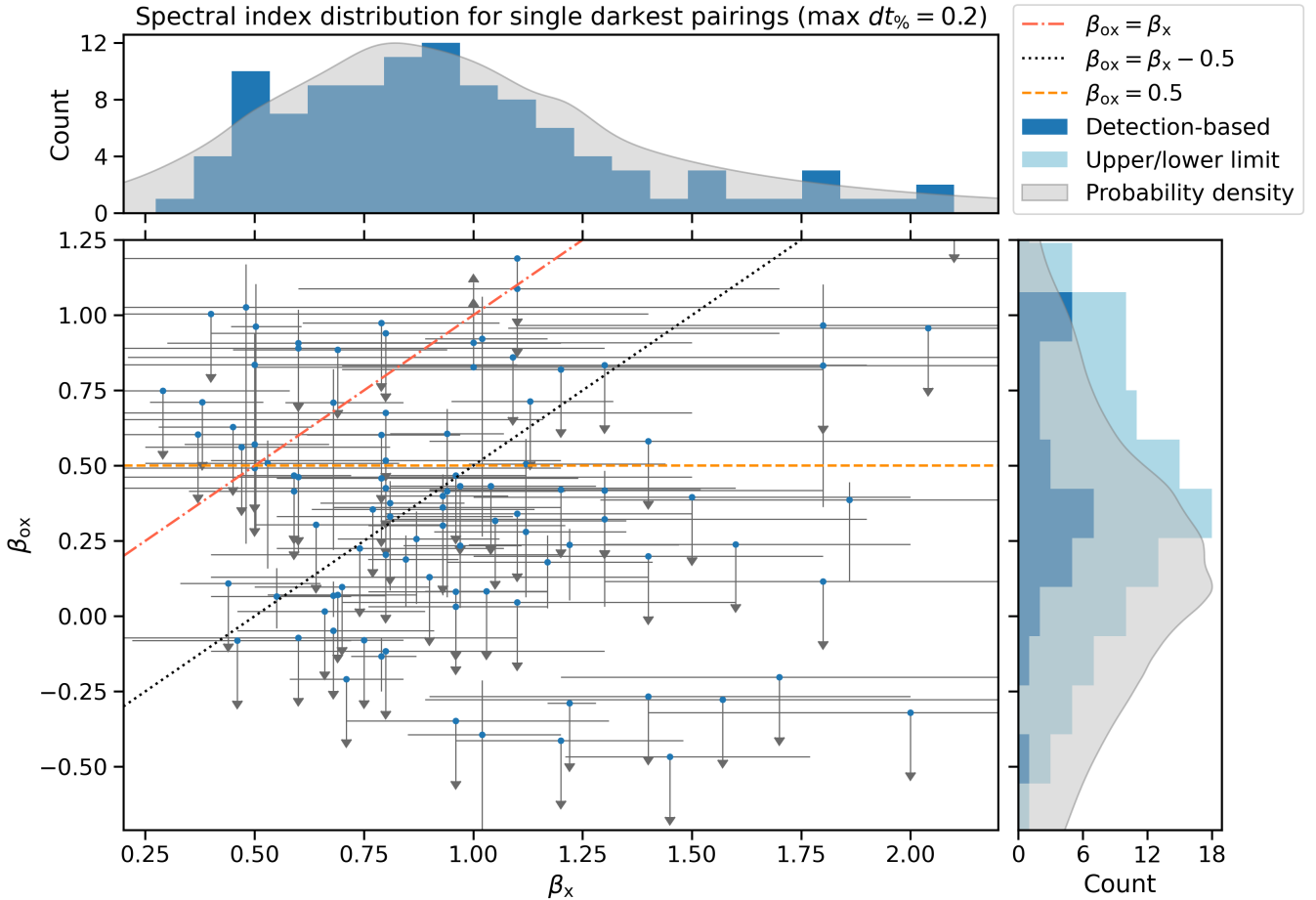
Figure 4. Each point in the plot above represents one unique burst and corresponds to the minimum value of β_{ox} for that GRB. Lines are drawn at various β_x–β_{ox} relations of interest (the van der Horst et al. definition of darkness is shown in dotted black, the Jakobsson et al. criterion is the dashed orange line, and the dash-dotted red line indicates $\beta_x = \beta_{ox}$). Top and side plots show distributions for each variable created by summing asymmetric split-normal probability distribution functions based on the error bars of each point along the respective axis (see §2.5).

T_{90}	dark at $\delta t > 5$ min	dark at any time	entire sample
> 20 s	7 (22 ± 9 %)	13 (41 ± 13 %)	32 (100%)
≤ 20 s	15 (10 ± 3 %)	38 (26 ± 5 %)	149 (100%)
> 2 s	11 (22 ± 7 %)	19 (38 ± 10 %)	50 (100%)
≤ 2 s	11 (8 ± 3 %)	32 (24 ± 5 %)	131 (100%)

Table 2. Number of optically dark GRBs, with (in parentheses) the fraction of the row total that each entry represents. Of note would be a rate that differs significantly for bursts above one of the T_{90} values versus below it. We show the breakdown using two different cutoff durations for defining EE bursts: $T_{90} = 2$ seconds, which is the classical criterion used for defining short bursts, and $T_{90} = 20$ seconds, which is the apparently more natural split in Fig. 6.

4.3 Meaningfully dark bursts

The early-time effect (discussed in §4.1) is so widespread that when we correct for it, we find only 4 bursts in our sample that exhibit meaningful optical darkness: GRBs 060121, 090423, 130603B, and 170728B.

4.3.1 GRB 060121

We find that GRB 060121 attains a minimum optical-to-X-ray spectral index of $\beta_{ox} \cong 0.18^{+0.09}_{-0.15}$ at $\delta t \approx 3.9$ hr (see Figure 7). Its most likely redshift is $z \sim 4.6$, with a possibility that it might be $z \sim 1.7$ (de Ugarte Postigo et al. 2006). Either way, this qualifies it as fairly high-redshift, especially for a short GRB. The Lyman-α forest, caused by clouds of neutral hydrogen in the intergalactic medium, can cause an extra absorption in the optical regime, possibly explaining the optical darkness of this GRB. However, if it is indeed at the higher redshift of ~4.6, corresponding to a Universe that is < 2 Gyr old, a BNS merger is an unlikely progenitor of this burst, and it may have resulted from a collapsar instead. This assumes a typical delay time for BNS mergers of 3–4 Gyr, as found by Wanderman & Piran (2015) and Skúladóttir & Salvadori (2020). However, Simonetti et al. (2019) have suggested a much faster timescale for BNS mergers, with an average coalescence time of 300–500 Myr. In this case, a merger-induced GRB is feasible at $z = 4.6$. Further compounding the uncertainty surrounding the origins of GRB 060121, Dichiara et al. (2021) find evidence that despite its prompt duration of $T_{90} = 1.97 \pm 0.06$ seconds, its lightcurve also exhibited extended emission, possibly hinting at a non-BNS progenitor as well.
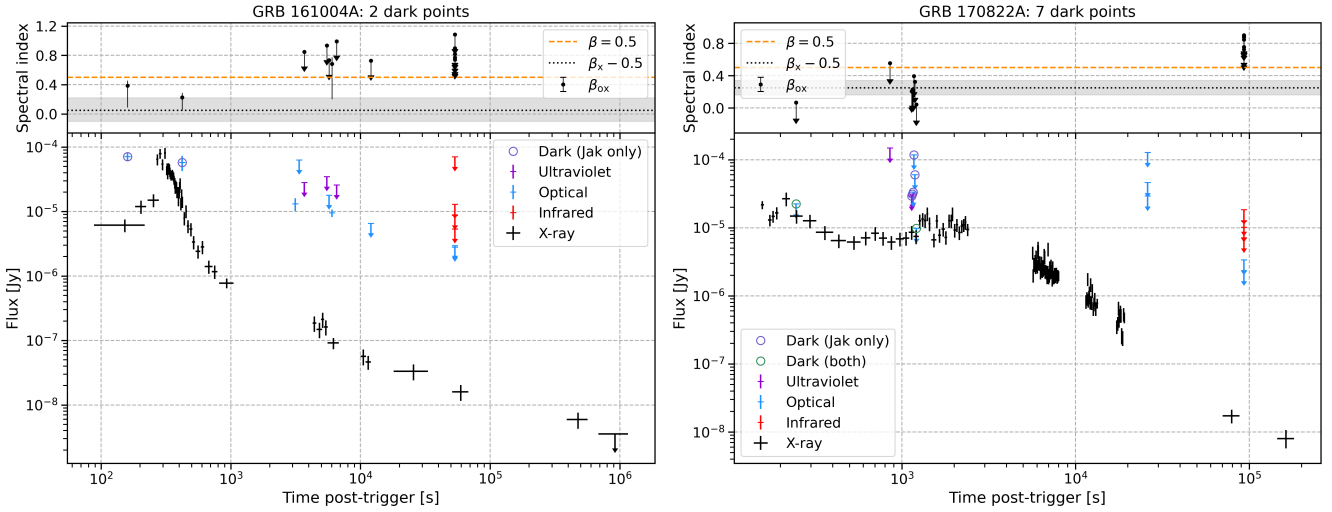
Figure 5. In the light curve of GRB 161004A on the left, we note an obvious X-ray flare (also flagged by the automated *Swift*-XRT light curve fitting routine; Evans et al. 2007, 2009) that peaks around $\delta t \approx 300$ seconds, causing optical points at $\delta t = 160$s and $\delta t \approx 420$s to appear dark, even though the optical behavior looks fairly canonical. Similarly, we observe plateau-like behavior (and possibly a flare) evident in the light curve of GRB 170822A on the right, lasting until around 2000 seconds post-trigger. Both are cases of anomalous X-ray behavior where it is clear that the light curve has not settled into 'normal' decay, meaning that standard assumptions about the optical and X-ray regimes existing as two regions of the same broadband spectrum are not valid.
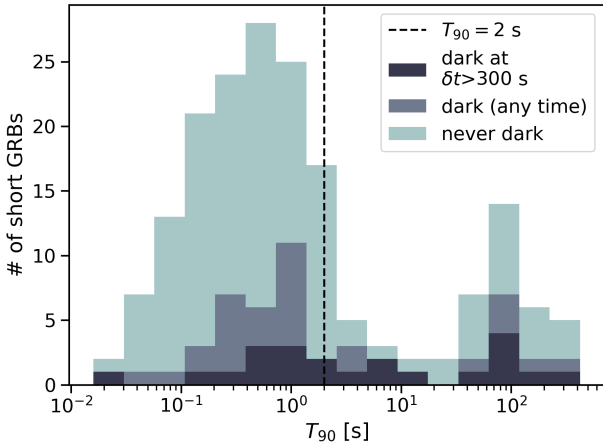

Figure 6. Histogram of T_{90} values for bursts in our sample. The vertical line shows $T_{90} = 2$s, the typically accepted value for defining the split between long- and short-duration GRBs. While the majority of events in our sample obey this, we also have some bursts that we deem to belong to the short class for other reasons and lie to the right of this dividing line. We note an apparent bimodality in this histogram, with the two peaks separated at $T_{90} \approx 20$s.

4.3.2 GRB 090423

GRB 090423 was and is one of the highest-redshift GRBs ever detected, at $z \sim 8.2$ (Tanvir et al. 2009; Salvaterra et al. 2009). Using a standard cosmological model (Bennett et al. 2014), this z corresponds to a cosmological age of only about 600 million years—over 13 billion years ago. Though it is darkest at early times ($\beta_{ox} < -0.21$ at $\delta t = 152$ s), the dark point at $\delta t \approx 55$ min is an upper limit of $\beta_{ox} < 0.38$ (see Figure 8). When the GRB was first detected, its initial classification as long or short was inconclusive. While the T_{90} duration (10.3 ± 1.1 seconds in the observer frame, 1.1 ± 0.1 seconds in the GRB rest frame), spectral lag, and peak energy were consistent with a short burst (Krimm et al. 2009; Zhang et al. 2009, explaining why it is present in our sample), it has since been confirmed to be
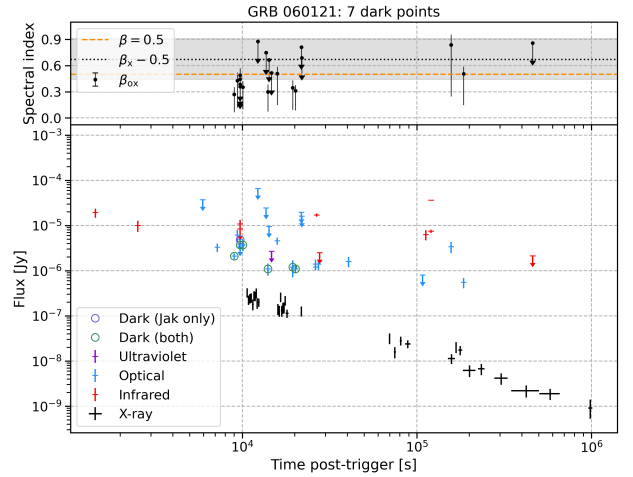

Figure 7. Multi-wavelength afterglow light curve of GRB 060121, showing optical darkness between approximately $1 \cdot 10^4$ and $2 \cdot 10^4$ seconds.

a high-redshift long GRB, which explains its optical darkness: at a redshift of $z \sim 8.2$, the Lyman-α forest would span wavelengths from 121.6 nm to 1119 nm, i.e., the entire optical regime.

4.3.3 GRB 130603B

With $T_{90} = 0.18 \pm 0.02$ seconds, GRB 130603B lies solidly in the short class of γ-ray bursts. Spectroscopic analysis by de Ugarte Postigo et al. (2014) assigns a redshift of $z \sim 0.36$, ruling out a high redshift as a viable explanation for optical darkness in this case. Of interest, however, is the late-time excess X-ray emission noted by Fong et al. (2014), which they attribute to a rapidly spinning supramassive magnetar merger product. Gompertz et al. (2014) supports the millisecond magnetar as a candidate central engine capable of producing both extended emission and a later-time X-ray plateau, with the extra emission powered by rotational spin-down. Fong et al.
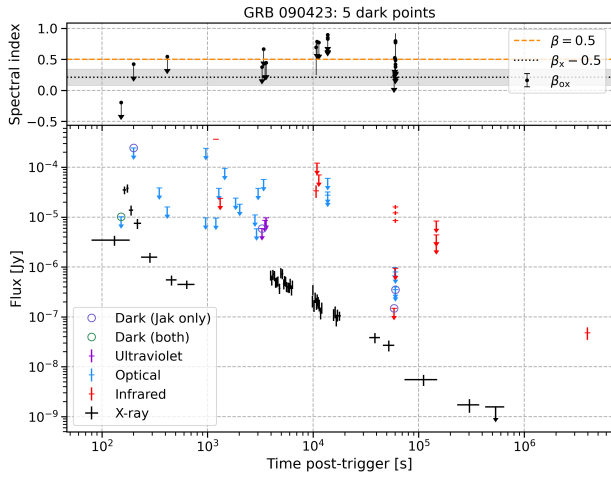
Figure 8. This light curve shows very early-time optical darkness in GRB 090423, possibly resulting from an apparent X-ray flare that peaks between 100 and 200 seconds. It is also dark at later times: in UV at $3 \cdot 10^3$ s, and in optical/nIR at $6 \cdot 10^4$ seconds.
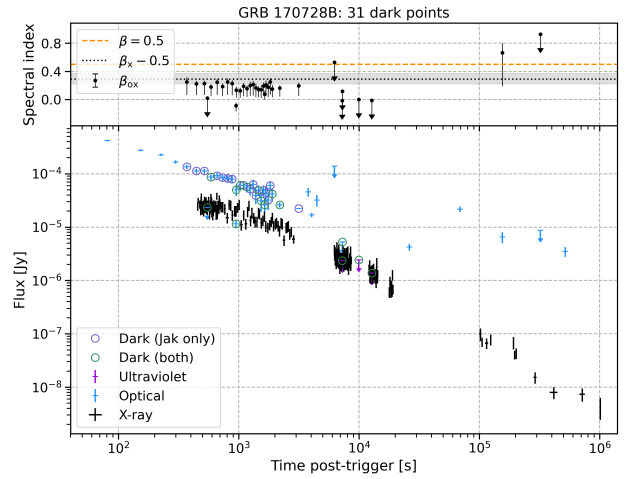

Figure 9. For GRB 130603B, we identify a cluster of optically dark data points around ~1 hour, around the time that Fong et al.'s magnetar model implies that excess X-ray emission becomes a significant contributor.

found that both the late-time ($\gtrsim 3 \cdot 10^3$ seconds) spectrum and the light curve of GRB 130603B were consistent with this model. In its light curve (Figure 9), we note that our optically dark points occur around this time as well: we find a minimum $\beta_{\mathrm{ox}} = 0.23^{+0.07}_{-0.21}$ at approximately 1 hour post-trigger. This indicates that the X-ray excess due to central engine activity may indeed be to blame for the shallow values of β_{ox}.

4.3.4 GRB 170728B

There is little published work on GRB 170728B. It is optically darkest at $t - t_0 = 16$ minutes with $\beta_{\mathrm{ox}} = -0.13^{+0.06}_{-0.11}$, but we also find an upper limit of $\beta_{\mathrm{ox}} < -0.014$ at ~ 3.5 hours. With a short, multi-peaked burst structure but a T_{90} of 47.7 ± 25.2 seconds (Ukwatta et al. 2017), this burst could be considered a short burst with extended emission, like those previously discussed in §4.2 (and is identified as such by Nugent et al. 2022). Fong et al. (2022) propose a host galaxy association with a spectroscopic redshift of $z = 1.272$. Optical

Figure 10. While the majority of the points that qualify GRB 170728B as optically dark occur at early times, there is also a cluster around 10^4 seconds.
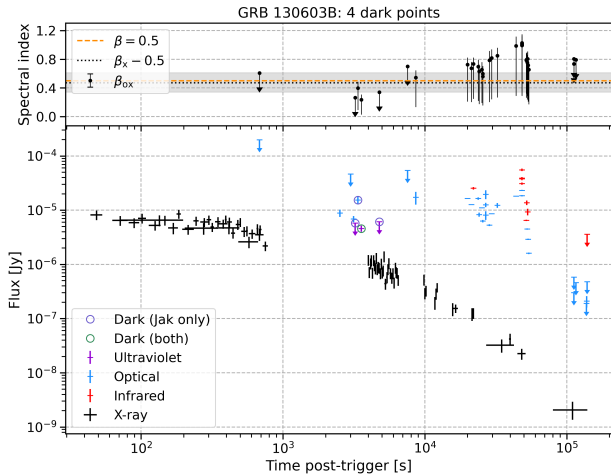
observations of GRB 170728B's afterglow that satisfy the criteria for optical darkness are available at a range of wavelengths across the optical range, with a majority of them (Dintinjana & Mikuz 2017) being in the R_c band ($\lambda_{\mathrm{eff}} \approx 636$ nm). This rules out redshift as a viable explanation for optical darkness in this case.

5 CONCLUSIONS

We present a complete, systematic study of optical darkness in short GRBs, a phenomenon that has until now only been studied extensively in long GRBs. To this end, we present our complete, scalable, and largely automated software pipeline, as well as a comprehensive catalog of short GRBs that comprises >3,000 optical observations and >5,500 X-ray data points from nearly 200 individual bursts.

Previous work on long GRBs has found a rate of optical darkness around half (Littlejohns et al. 2015, and references therein). While our initial result for short GRBs is consistent with this, many instances of optical darkness in our sample stem from early-time observations, and we determine that in most cases an excess of X-ray emission is to blame rather than any significant optical deficit. The classification of data points as optically dark or not depends heavily on how quickly follow-up observations are obtained, and assessing optical darkness using existing criteria is better done at later times once X-ray emission has settled into regular decay. The high rate of occurrence of anomalous early-time X-ray behavior suggests that the standard assumption of a purely synchrotron afterglow with one broadband emission component is not a complete picture. While previous studies of optical darkness in long GRBs have avoided this problem by using data obtained at later times, the comparatively faint overall nature of short GRB afterglows means that the availability of data skews earlier and identifying true optical darkness is more difficult.

When we account for early-time effects, we find that, as expected, optical darkness is much more rare in short GRBs than in long ones. We identify only 4 of our GRBs that are optically dark after the X-ray lightcurve has entered regular decay, and one of them is actually a long GRB. Because our eligible sample (of bursts with temporally-matched data) consists of 108 GRBs, this number represents a *true* optical darkness rate of less than 3%. To explain the optical darkness in these few individual cases, we turn to redshift, late-time X-ray

excess, or the possibility of heterogeneity in short GRB progenitors, remnants, and environments that could cause discrepant afterglow behavior.

The tools and results presented here are structured so as to make updating and keeping the catalog up to date as straightforward as possible. In addition to newly developed computational tools with wide-ranging cross-disciplinary applicability, this work provides a robust framework for further investigation and analysis of optical darkness in both long and short GRBs.

ACKNOWLEDGEMENTS

DATA AVAILABILITY

The complete datasets underlying this article are available on GitHub, in the repository cgobat/dark-GRBs. The data were derived from sources in the public domain: UKSSDC, the GCN Circulars Archive, and previously published works (Fong et al. 2015; Rastinejad et al. 2021, among others).

REFERENCES

Astropy Collaboration et al., 2013, A&A, 558, A33
Astropy Collaboration et al., 2018, AJ, 156, 123
Beniamini P., Piran T., 2019, MNRAS, 487, 4847
Bennett C. L., Larson D., Weiland J. L., Hinshaw G., 2014, ApJ, 794, 135
Berger E., 2010, ApJ, 722, 1946
Burrows D. N., et al., 2005, Space Sci. Rev., 120, 165
Covino S., et al., 2013, MNRAS, 432, 1231
Dichiara S., et al., 2021, ApJ, 911, L28
Dintinjana B., Mikuz H., 2017, GRB Coordinates Network, 21394, 1
Eichler D., Livio M., Piran T., Schramm D. N., 1989, Nature, 340, 126
Evans P. A., et al., 2007, A&A, 469, 379
Evans P. A., et al., 2009, MNRAS, 397, 1177
Fong W., et al., 2014, ApJ, 780, 118
Fong W., Berger E., Margutti R., Zauderer B. A., 2015, ApJ, 815, 102
Fong W., et al., 2022, ApJ, 940, 56
Fynbo J. U., et al., 2001, A&A, 369, 373
Gehrels N., Ramirez-Ruiz E., Fox D. B., 2009, ARA&A, 47, 567
Gobat C., 2022, Asymmetric Uncertainty, Astrophysics Source Code Library (ascl:2208.005), http://ascl.net/2208.005
Gompertz B. P., O'Brien P. T., Wynn G. A., 2014, MNRAS, 438, 240
Gompertz B. P., Levan A. J., Tanvir N. R., 2020, ApJ, 895, 58
Greiner J., et al., 2011, A&A, 526, A30
Groot P. J., et al., 1998, ApJ, 493, L27
Jakobsson P., Hjorth J., Fynbo J. P. U., Watson D., Pedersen K., Björnsson G., Gorosabel J., 2004, ApJ, 617, L21
John S., 1982, Communications in Statistics - Theory and Methods, 11, 879
Kouveliotou C., Meegan C. A., Fishman G. J., Bhat N. P., Briggs M. S., Koshut T. M., Paciesas W. S., Pendleton G. N., 1993, ApJ, 413, L101
Krimm H. A., Norris J. P., Ukwatta T. N., Barthelmy S. D., Evans P. A., Gehrels N., Stamatikos M., 2009, GRB Coordinates Network, 9241, 1

GRB	T_{90} [sec]	X-ray	Optical	Temporal matches	Dark
211227A	83.792	101	22	86	83
211106A	1.75	4	13	1	0
211023B	1.296	19	39	32	2
210919A	0.164	2	35	2	0
210726A	0.388	15	5	2	1
...	...	...	...	...	...
050906	0.064	1	1	0	0
050813	0.448	2	12	0	0
050724	95.964	238	7	55	0
050509B	0.048	3	1	0	0
050202	0.112	0	1	0	0

Table A1. Number of available data points for each of the short GRBs in our sample, along with the number of temporally-matching points and the resulting number of points that qualify as 'dark' by one or both of the two methods described above.

Only a portion of this table is shown here to demonstrate its form and content. A machine-readable version of the full table is available.

LIGO Scientific Collaboration et al., 2017, ApJ, 848, L12
Lazzati D., Covino S., Ghisellini G., 2002, MNRAS, 330, 583
Liang E. W., et al., 2006, ApJ, 646, 351
Lien A., et al., 2016, ApJ, 829, 7
Littlejohns O. M., et al., 2015, MNRAS, 449, 2919
Masetti N., et al., 2001, A&A, 374, 382
Norris J. P., Bonnell J. T., 2006, ApJ, 643, 266
Nousek J. A., et al., 2006, ApJ, 642, 389
Nugent A. E., et al., 2022, ApJ, 940, 57
O'Connor B., et al., 2022, MNRAS, 515, 4890
Rastinejad J. C., et al., 2021, ApJ, 916, 89
Rol E., Wijers R. A. M. J., Kouveliotou C., Kaper L., Kaneko Y., 2005, ApJ, 624, 868
Roming P. W. A., et al., 2005, Space Sci. Rev., 120, 95
Salvaterra R., et al., 2009, Nature, 461, 1258
Schlafly E. F., Finkbeiner D. P., 2011, ApJ, 737, 103
Simonetti P., Matteucci F., Greggio L., Cescutti G., 2019, MNRAS, 486, 2896
Skúladóttir Á., Salvadori S., 2020, A&A, 634, L2
Stanek K. Z., et al., 2001, ApJ, 563, 592
Tanvir N. R., et al., 2009, Nature, 461, 1254
Troja E., King A. R., O'Brien P. T., Lyons N., Cusumano G., 2008, MNRAS, 385, L10
Ukwatta T. N., et al., 2017, GRB Coordinates Network, 21384, 1
Wanderman D., Piran T., 2015, MNRAS, 448, 3026
Woosley S. E., 1993, ApJ, 405, 273
Zhang B., et al., 2009, ApJ, 703, 1696
Zheng Z., Ramirez-Ruiz E., 2007, ApJ, 665, 1220
de Ugarte Postigo A., et al., 2006, ApJ, 648, L83
de Ugarte Postigo A., et al., 2014, A&A, 563, A62
van Paradijs J., et al., 1997, Nature, 386, 686
van der Horst A. J., Kouveliotou C., Gehrels N., Rol E., Wijers R. A. M. J., Cannizzo J. K., Racusin J., Burrows D. N., 2009, ApJ, 699, 1087

APPENDIX A: SUPPLEMENTARY TABLES

Table A1 contains a summary of the available data, matches, and optical darkness results for each GRB in our sample.

This paper has been typeset from a TeX/LaTeX file prepared by the author.